Water vapor increase in the northern lower stratosphere by the Asian monsoon anticyclone observed during TACTS/ESMVal campaigns

Christian Rolf[1], Bärbel Vogel[1], Peter Hoor[2], Armin Afchine[1], Gebhard Günther[1], Martina Krämer[1], Rolf Müller[1], Stefan Müller[2,3], Nicole Spelten[1], and Martin Riese[1]

[1]Institute for Energy and Climate research (IEK-7), Forschungszentrum Jülich GmbH, Jülich, Germany.
[2]Institute for Atmospheric Physics, Johannes Gutenberg University, Mainz, Germany.
[3]now at: Enviscope GmbH, 60489 Frankfurt, Germany.

Correspondence to: C. Rolf (c.rolf@fz-juelich.de)

Abstract. The impact of air masses from Asia influenced by the Asian monsoon anticyclone on the northern hemispheric stratosphere is investigated based on in-situ measurements. An statistical significant increase in water vapor of about 0.5 ppmv (11 %) and methane up to 20 ppbv (1.2 %) in the extra-tropical stratosphere above a potential temperature of 380 K was detected between August and September 2012 by in-situ instrumentation in the northern hemisphere during the HALO aircraft mission TACTS and ESMVal. We investigate the origin of this water vapor and methane increase with the help of the three-dimensional Lagrangian chemistry transport model CLaMS. We assign the source of the moist air masses in the Asian region (North and South India, East China, South East Asia and tropical Pacific) based on tracers of airmass origin used in CLaMS. The water vapor increase is correlated to an increase of the simulated Asian monsoon air mass contribution from 10 % in August to 20 % in September, which corresponds to a doubling of the influence of air masses affected by the Asian monsoon region. Additionally, back trajectories starting at the aircraft flight paths are used to differentiate between transport from the Asian monsoon anticyclone and other source regions by calculating the Lagrangian cold point (LCP). The geographic location of the LCPs, which indicates the region where the imprint of water vapor concentration along these trajectories occur, can be exclusively attributed to the Asian monsoon region.

1 Introduction

Radiatively active trace gases like water vapor and methane play a key role in determining the radiative balance in the upper troposphere and lower stratosphere (UTLS) and thus impact the surface climate of the Earth (*Forster and Shine*, 2002; *Riese et al.*, 2012). Here we focus on transport pathways and exchange processes between troposphere and stratosphere to better understand the variability of water vapor and methane in this climatically sensitive region of the atmosphere.

In general, freeze-dried air masses with a low amount of water vapor enter the stratosphere in the tropical tropopause layer (TTL) and are transported vertically via the Brewer-Dobson circulation (BDC) deep into the stratosphere and quasi-horizontally into the extra-tropical lower stratosphere (Ex-LS) (e.g. *Gettelman et al.*, 2011). Thus, the air in the Ex-LS constitutes a mixture

Atmospheric
Chemistry
and Physics
Discussions

of young air-masses originating from quasi-horizontal transport out of the TTL and old stratospheric air in the downwelling branch of the BDC (e.g. *Bönisch et al.*, 2009; *Ploeger et al.*, 2013; *Vogel et al.*, 2016). In general, increasing inflow of tropospheric air masses from the tropics in combination with higher values along the history of air mass temperature cause a moistening of the Ex-LS in summer compared to winter months (e.g. *Hoor et al.*, 2005; *Krebsbach et al.*, 2006; *Ploeger et al.*,

5 2013; *Zahn et al.*, 2014). In addition, the Asian monsoon anticyclone (AMA) is linked to convection and thus rapid vertical transport of surface air from India and east Asia which facilitates transport of young and moist air masses from the upper troposphere into the northern extra-tropical stratosphere (e.g. *Dethof et al.*, 1999; *Vogel et al.*, 2014, 2015). This additional transport pathway leads to a moistening of the northern Ex-LS (e.g. *Müller et al.*, 2016; *Vogel et al.*, 2016).

Air masses within the Asian monsoon upper-tropospheric anticyclone are confined horizontally by a transport barrier char-

10 acterized by a potential vorticity (PV) gradient (*Ploeger et al.*, 2015). This confinement is responsible for an enrichment of tropospheric constituents and higher amounts of water vapor or methane (e.g. *Park et al.*, 2004, 2007; *Randel and Park*, 2006; *Schuck et al.*, 2010; *Patra et al.*, 2011; *Baker et al.*, 2012; *Bian et al.*, 2012; *Pan et al.*, 2016; *Santee et al.*, 2017). A horizontal transport pathway out of the anticyclone is directed westerly into the tropical tropopause layer (TTL) (*Popovic and Plumb*, 2001). A second pathway of these moist and polluted air masses exists, where air from the AMA is transported to the east along

15 the subtropical jet and subsequently transport into the northern lower stratosphere via Eddy shedding followed by tropopause crossing (e.g. *Dethof et al.*, 1999; *Hsu and Plumb*, 2000; *Vogel et al.*, 2014, 2016). These frequent occurring Eddy shedding events triggered by Rossby wave activity flood the northern extra-tropical lower stratosphere with tropospheric air masses from the Asian subcontinent (e.g. *Müller et al.*, 2016; *Vogel et al.*, 2014, 2016). Also, from AURA-MLS satellite observations it is shown that the Asian monsoon is hydrating the northern stratosphere (*Uma et al.*, 2014).

20 The influence of the Asian monsoon on the Ex-LS is from observational point of view mostly analyzed based satellite limb sounder measurements, which have only limited vertical resolution typically larger than 1-2 km in the lowermost stratosphere (*Hegglin et al.*, 2013). Here, we present in-situ water vapor and methane measurements in the northern lower stratosphere performed in August and September 2012. We investigate changes of these trace gases during the observational time period and attribute these changes to transport from the Asian monsoon region by using Lagrangian back-trajectory analysis in com-

25 bination with artificial tracers of airmass origin.

2 Methods and Instruments

This study bases on data collected during the two aircraft campaigns TACTS (Transport and Composition in the UT/LMS) and ESMVal (Earth System Model Validation). These campaigns were conducted between August and October 2012 mainly in the northern hemisphere in the region from the Cape Verde Islands to the Arctic, mainly over Europe and the Atlantic Ocean. The

30 data are split into two time periods. These two periods, referred to as phase 1 and phase 2 hereafter, cover the time period from August 28 to September 5 and September 18 until September 26, 2012, respectively. More information about the data coverage can be found in *Müller et al.* (2016). The separation allows the temporal evolution of the trace gas composition of the Ex-LS between the two phases to be investigated. In the following, the water vapor and methane instruments aboard the HALO

aircraft are briefly described. In addition, we used CLaMS (Chemical Lagrangian Model for the Stratosphere) model results interpolated onto the flightpath and also CLaMS backward trajectory calculations from the measurement location as described further below.

2.1 Measurements of water vapor

5 The water vapor data used in this study were measured with the FISH (Fast In-situ Stratospheric Hygrometer) instrument. The measurement technique bases on Lyman-α photofragment fluorescence and is suitable for measuring water vapor in the range of 1 to 1000 ppmv (*Zöger et al.*, 1999). The FISH is a well-established closed-path hygrometer with a long history in aircraft measurements and instrument intercomparisons (*Meyer et al.*, 2015). Calibrations are performed during the campaigns with a MBW DP30 frost point hygrometer achieving a accuracy of $6\% \pm 0.4$ ppmv at a time resolution of 1 Hz during
10 TACTS/ESMVal.

2.2 Measurements of methane

The methane data are obtained by the TRIHOP instrument. The measurement technique bases on infrared absorption spectroscopy with a three channel quantum cascade laser spectrometer capable of measuring CO, CO_2, N_2O and CH_4. An in-situ calibration against a secondary standard traceable to the NOAA scale was applied during the campaign. TRIHOP methane data
15 are available every eight seconds with an integration time of 1.5 seconds, a precision of 9.5 ppbv (2σ) and an uncertainty of 13.5 ppbv relative to the standard. For more details see *Müller et al.* (2016).

2.3 CLaMS simulations with artificial air mass origin tracers

In this study, we use the three-dimensional chemistry transport model CLaMS (*McKenna et al.*, 2002a, b; *Pommrich et al.*, 2014, and references therein) with the setup described in *Vogel et al.* (2015). The simulations covered the time period from
20 May 1 to October 31, 2012, capture the Asian monsoon season in 2012.

The CLaMS simulation, used here, is driven by ERA-Interim meteorological fields (*Dee et al.*, 2011) from the ECMWF (European Centre for Medium-Range Weather Forecasts) and covers the atmosphere from the surface up to 900 K potential temperature (≈ 37 km altitude) with a vertical resolution of 400 m around the tropopause. In the simulation, "emission tracers" are released in the boundary layer ($\approx$ 2-3 km above surface) which globally marks all regions of the Earth surface. These
25 different artificial tracers are freshly emitted every 24 h in the boundary layer and their concentrations in the atmosphere represents the airmass contributions from the respective source regions. For more details see *Vogel et al.* (2015, 2016).

Vogel et al. (2015) showed that the emission tracers for India and eastern China are correlated to AURA-MLS (*Livesey et al.*, 2011) satellite measurements of potential vorticity (PV), O_3, and CO. Thus, they can be used as proxy for the location and shape of the AMA and allow for transport studies of air masses from the AMA into the northern extra-tropical lower
30 stratosphere. In addition, emission tracer from southeast Asia and Pacific Ocean contribute to the airmass composition of the outer edge of the AMA. Thus, to study the transport of Asian monsoon affected air masses, the most important emission regions

Table 1. Latitude and longitude range of artificial boundary layer sources in the CLaMS model, which are used to define the "Asian monsoon surface tracer" (MON).

Emission tracer	Latitude	Longitude
Northern India (NIN)	20-40°N	55-90°E
Southern India (SIN)	0-20°N	55-90°E
Eastern China (ECH)	20-40°N	90-125°E
Southeast Asia (SEA)	12-20°N	90-155°E
Tropical Pacific Ocean (TPO)	20°S-20°N	55°E-80°W

are India/China, southeast Asia, and the tropical Pacific Ocean. The sum of all these model boundary layer tracers is referred to as "Asian monsoon surface tracer" (MON) (see Table 1). This tracer marks young air masses that are confined during summer in the AMA and air masses from southeast Asia and the tropical Pacific Ocean influenced by the large-scale flow around the anticyclone in the UTLS. All other source regions can be neglected, since it is shown in *Vogel et al.* (2016), that these regions

5   do not significantly contribute to flooding of the lower stratosphere with young tropospheric air masses in summer and autumn 2012.

2.4 Airmass trajectory calculations

In contrast to three-dimensional CLaMS simulations, pure trajectory calculations do not account for mixing. However, the position of an air parcel and the temperature development along the trajectory can be tracked over several days or weeks.

10   The airmass trajectories are calculated by means of the trajectory module of CLaMS 50 days backward in time from every 10th second from the location of the flightpath using ERA-Interim data (*Dee et al.*, 2011) of the ECMWF. The trajectories are based on the horizontal wind fields and diabatic heating rates with a resolution of 1° x 1° with 60 vertical levels from the surface up to 0.1 hPa. Additional parameters like temperature, pressure, and potential vorticity (PV) are interpolated from the ERA-Interim data onto the trajectories. In addition, the local distance to the thermal tropopause (WMO) is calculated for each

15   trajectory time step and added to the trajectory data (e.g. *Krebsbach et al.*, 2006). The water vapor saturation mixing ratio with respect to ice (hereafter: saturation mixing ratio) along the trajectories is calculated based on the actual trajectory temperature. The Lagrangian cold point (LCP) is defined by the minimum of the temperature along the trajectory and thus minimum of the saturation mixing ratio. With these parameters pure stratospheric trajectories can be separated from trajectories with tropospheric origin within the last 50 days by comparing the distance to the tropopause before and after the LCP. All trajectories

20   with a negative/positive distance to the thermal tropopause before/after the LCP passed the tropopause from the troposphere into the stratosphere and represent air masses which originate in the troposphere.

Atmospheric
Chemistry
and Physics
Discussions

3 Results

The main purpose of this study is to corroborate the hypothesis that air masses from Asia and the tropical Pacific affected by the AMA are the main source of the moistening found in the Ex-LS in late summer and fall in the northern hemisphere. First, we present in-situ water vapor measurements of the two phases (August and September) and reinforce the hypotheses based

5   on water vapor - methane correlations. Second, to finally confirm the hypothesis we combine the measurements with CLaMS model results and the 50-day backward trajectory analysis.

3.1 Moistening the Ex-LS

Water vapor is strongly coupled to the temperature history of an airmass. Therefore, we choose in the following the distance to the local thermal tropopause as the vertical coordinate in units of potential temperature. In Figure 1 a and b we display the

10   mean water vapor distributions of both phases (phase 1 and phase 2) along equivalent latitude. High water vapor values (> 10 ppmv), representing moist tropospheric or tropospheric influenced air, can be found below and up to 20 K above the thermal tropopause during both phases. Dryer air masses down to the stratospheric background level of 4-5 ppmv are observed 30 to 90 K above the thermal tropopause. In phase 1, the dryer air masses are observed closer to the thermal tropopause, while in phase 2 such dry air masses are found at 10 K higher potential temperatures. Both distributions have a similar vertical and

15   horizontal extent and thus the difference between both phases reveals local changes of water vapor mixing ratios over the time period (see Fig. 1c). Air masses with PV < 8 PVU reveal a large variability between phase 2 and phase 1, which is most likely due to local variability of water vapor, the thermal tropopause and planetary wave activity which distort the location of the sub-tropical jet core. *Kunz et al.* (2015) showed that the climatological transport barrier between tropospheric and stratospheric air masses is located at a PV value of 7-8 PVU in the time between June-November in the northern hemisphere. Thus, we will

20   focus on air masses with PV > 8 PVU in the following analysis, since these air masses are not affected by small scale mixing processes directly at the tropopause.

All air masses with PV values larger than 8 PVU show a distinct 5-10 % increase of water vapor in phase 2 compared to phase 1. The occurrence of these air masses range from 40°N to 75°N in equivalent latitude horizontally and corresponds to potential temperatures larger than 380 K. The frequency distributions of those water vapor values with PV values larger

25   than 8 PVU allow us to quantify the strength of moistening between both phases (see Fig. 1d). The distribution of phase 1 is very compact with a mean water vapor concentration of 4.5 ppmv, while the distribution of phase 2 is shifted to higher water vapor concentration with a mean value of 5 ppmv and shows a tail towards higher water vapor mixing ratios. The difference in the mean water vapor concentration indicates a statistic significant moistening of the Ex-LS of about 0.5 ppmv within a time period of less than a month. This finding is in accordance with CLaMS model simulations and MLS satellite measurements

30   which show in the time period from May to November an increase of mean water vapor mixing ratio in the northern Ex-LS by 1.5 ppmv (1.0 ppmv) at 380 K (400 K) due to transport of air masses originating from source regions in Asia (see page 15316 in *Vogel et al.*, 2016). In addition to the measured increase in mean water vapor of 0.5 ppmv a mean increase of 20 ppbv methane is observed in the same time period (not shown).
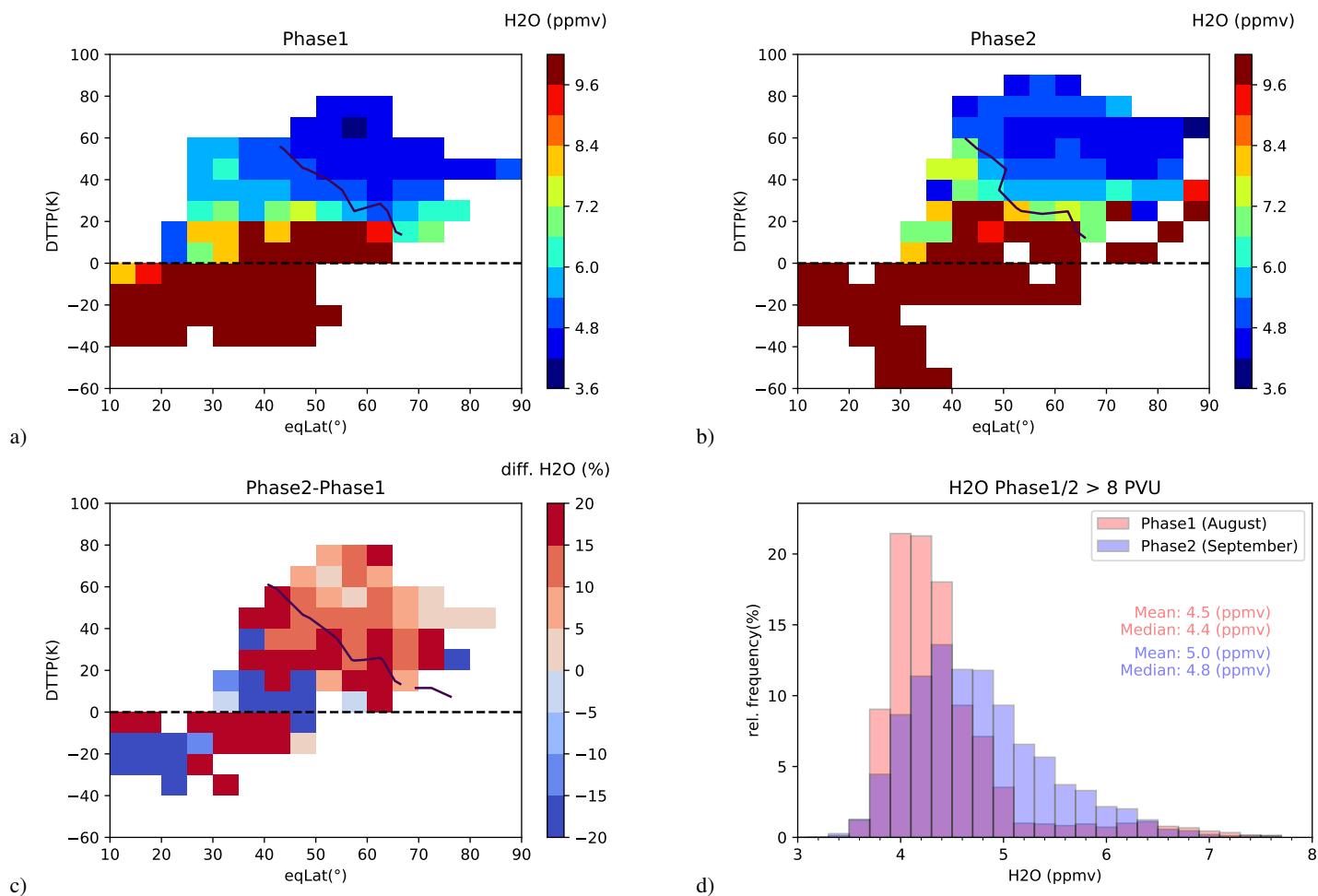
Figure 1. Mean distribution of H_2O as a function of equivalent latitude and distance to thermal tropopause (DTTP) in potential temperature units: a) phase 1 b) and phase 2. c) Relative differences of H_2O between phase 2 and phase 1. The dashed and the solid black line represents the thermal tropopause and the 8 PVU isoline, respectively. d) Frequency distribution of H_2O for the lower stratosphere (PV > 8 PVU) for phase 1 (red) and phase 2 (blue). The mean and median values of each distribution given in red and blue, respectively.

3.2 Tracer of airmass origin

Our simulations of corresponding artificial air mass origin tracers (Figures 2 a, b) indicate that the observed moistening during phase 2 is the result of an increase of airmass contribution from the Asian monsoon region. MON increased relatively by about 20 to 100 % from phase 1 to phase 2 above the 8 PVU level, which corresponds nearly to a doubling (see Fig. 2 c). The increase

5 of MON in this altitude range is correlated with the observed increase in water vapor between both phases. The frequency distributions in Figures 2 d) reveal the clear shift of MON to higher values, where the mean values show an increase of 8.6 % from phase 2 to phase 1. In particular, there is only a slight increase of surface tracers (∼1 %) from other locations (residual
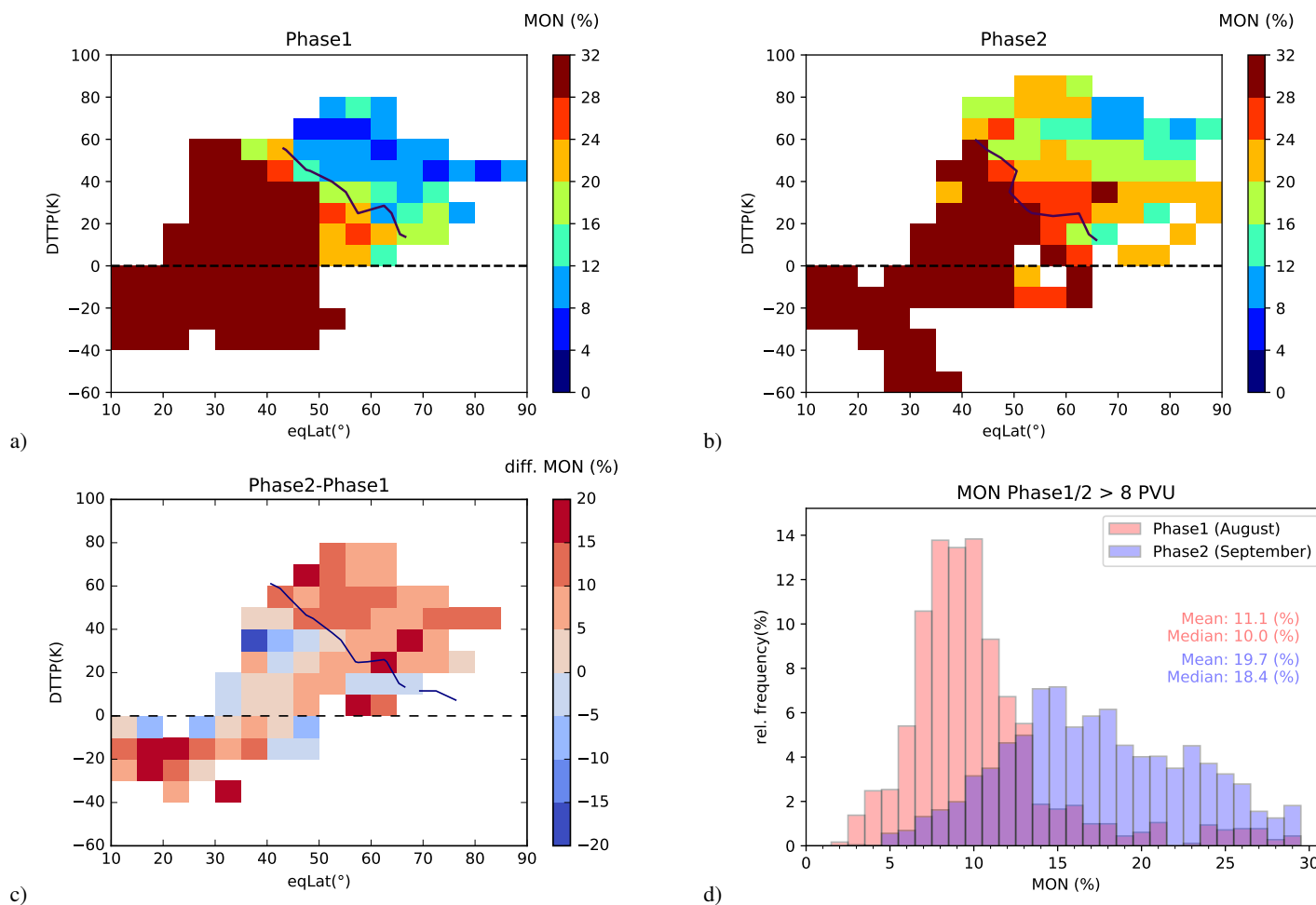
Figure 2. Same as Figure 1 but for the simulated Asian monsoon surface tracer MON.

surface without the monsoon region, MON) in the same time period. Therefore, the moistening of 0.5 ppmv can be related to the increase of MON by 8.6 %.

3.3 Water vapor - methane correlation

The correlation of observed water vapor with observed methane provides further evidence on the large air mass contribution

5 of the Asian monsoon region. Methane has its sources at the Earth's surface and thus has the highest concentrations in the troposphere. Methane concentrations are especially high in regions with large industrial activity or natural out-gassing from wetlands like rice cultivation in India / Southeast Asia (*Park et al.*, 2004; *Xiong et al.*, 2009). In the stratosphere, the methane concentration decreases with altitude due to oxidization. Thus, methane is suitable as a monsoon specific tropospheric tracer, in particular for the Asian monsoon regions because of high emissions on the ground and strongly enhanced concentrations in

Atmospheric
Chemistry
and Physics
Discussions
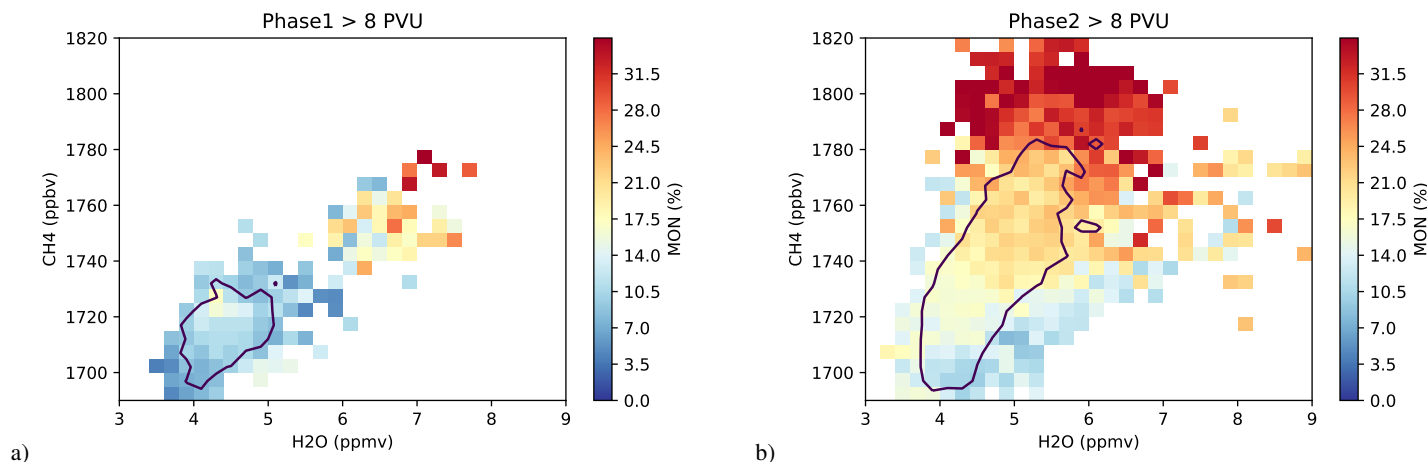
Figure 3. Correlation of water vapor and methane for PV > 8 PVU, color-coded by the Asian monsoon surface tracer MON. The solid black line represents the core region which contains 75 % of the data.

the AMA compared to the free troposphere as shown by measurements of CARIBIC (*Schuck et al.*, 2010; *Patra et al.*, 2011; *Baker et al.*, 2012).

Figure 3 shows the correlations of measured water vapor and methane mixing ratios in the lower stratosphere (PV > 8 PVU) for the both phases. The correlation in phase 1 is compact with nearly no statistical significant enhancements in methane and water vapor compared to the background concentrations in the lower stratosphere (*Zahn et al.*, 2014). The core region of the scatter plot defined by the 75 % percentile of the frequency distribution (black contour) ranges from around 3.8 to 5.1 ppmv in water vapor and from 1700 to 1730 ppbv in methane. The amount of MON is relatively low with values around 12 % in the core region. Only few measurements with high MON values up to 30 % are found, showing the highest water vapor and methane values in phase 1. In contrast, the correlation in phase 2 is dominated by measurements with higher methane and water vapor concentrations. The core region of the data ranges from 1700 to 1790 ppbv in methane and 3.7 to 6.2 ppmv in water vapor. The amount of MON is in general significantly higher in phase 2 compared to phase 1 and increases strongly up to 30 % in phase 2. The increase in water vapor and methane concentration is statistically correlated with the increase in MON. In fact, the slope of the correlation is tilted towards higher methane and water vapor concentrations in phase 2, which confirms the influence of methane-rich tropospheric air masses from the Asian monsoon region in the Ex-LS.

3.4 Lagrangian cold point from backward trajectories

The amount of water vapor which is transported from the troposphere into the stratosphere is strongly coupled with the Lagrangian cold point (LCP), where typically the water vapor is dehydrated close to the saturation mixing ratio by ice crystal formation and subsequent sedimentation (e.g. *Schoeberl and Dessler*, 2011). Thus, the amount of water vapor in these air

Atmospheric
Chemistry
and Physics
Discussions

masses is nearly preserved after passing the LCP in the tropical, sub-tropical and mid-latitude stratosphere. The geographic location of the LCP along the backward trajectory marks the location of the imprint on water vapor concentration.

Vogel et al. (2016) showed that Eddy shedding and in-mixing of tropospheric air-masses can occur at potential temperatures around 380 K directly between double tropopause features passing the transport barrier at the climatological jet core. However,

5   the locations of LCPs in case of Eddy shedding events do not implicitly coincide with the point of in-mixing into the Ex-LS. In this case the locations of LCPs are typically at the top of the upwelling in the region of the AMA, whereas in-mixing into the Ex-LS can be found at locations where Rossy wave breaking occurs easterly or westerly of the AMA along the subtropical jet.

In the following, all backward trajectories for air parcels with PV > 8 PVU according to Section 3.1 are considered (i.e. 2909 out of 11333 (25.6 %) trajectories for phase 1 and 7301 out of 14673 (49.8 %) trajectories for phase 2). The LCPs (see Figure

10   4 a-b) are mostly located in the subtropics with equivalent latitudes ranging from 0 to 50°N. Notably, they cluster meridionally above India/China/Indonesia, North America, and West/North Africa in both phases. Interestingly, all these regions can be assigned to respective monsoon systems over Asia, America and Africa. In phase 1, only 158 out of 2909 (5.4 %) trajectories with PV > 8 PVU are classified as tropospheric with the LCP criteria above, i.e. more trajectories are entirely in the stratosphere. Furthermore, phase 2 reveals more frequent LCP occurrence with 846 out of 7301 (11.6 %) trajectories with PV > 8 PVU in

15   these regions. In addition, phase 2 also shows a clear increase of LCP's in the region of India/China/Indonesia compared to phase 1. The relative difference between phase 2 and phase 1, normalized to all trajectories (tropospheric and stratospheric), further confirms this (see Figure 4c). The signal of the two other monsoon circulations i.e. the American monsoon and the African Monsoon vanishes in this analysis. The dominant appearance of LCP's in the Asian monsoon region is obvious. Thus, the Asian monsoon has the most frequent LCP occurrence, the largest extent, and thus largest impact on stratospheric water

20   vapor enhancements in the observed time period.

The selection criterion for trajectories described in Section 2.4 can be used to quantify the amount of trajectories which stayed in the stratosphere for at least 50 days (stratospheric origin) or passed the LCP from troposphere into the stratosphere (tropospheric origin) as shown in Figure 5. In phase 1 the fraction of flightpath back-trajectories with tropospheric origin ($p1t$) is 5.4 % (94.6 % stratospheric, $p1s$), while in phase 2 11.6 % ($p2t$) had a tropospheric origin (88.4 % stratospheric, $p2s$). The

25   larger amount of tropospheric origin trajectories corroborate the existence of stronger troposphere to stratosphere exchange in phase 2. The increase of mean water vapor from phase 1 (4.5 ppmv) to phase 2 (5.0 ppmv) by the Asian monsoon trajectories can be calculated with a system of linear equations:

$$\begin{pmatrix} p1t & p1s \\ p2t & p2s \end{pmatrix} \begin{pmatrix} wv_1 \\ wv_2 \end{pmatrix} = \begin{pmatrix} 4.5\text{ppmv} \\ 5.0\text{ppmv} \end{pmatrix} \quad \Rightarrow \quad wv_1 = 4.1\text{ppmv}, wv_2 = 11.9\text{ppmv} \tag{1}$$

Here wv_1 denotes the water vapor background mixing ratio and wv_2 the water vapor contribution from the monsoon tra-

30   jectories. From this simple calculation, it can be concluded that the observed increase in the mean water vapor concentration of 0.5 ppmv between both phases (see Figure 1d) can be attributed to transport of moist tropospheric air masses with a mean water vapor concentration of about 12 ppmv compared to a stratospheric background of 4.1 ppmv. These values fit quite well

to CLaMS model simulations in *Vogel et al.* (2016) who found a stratospheric background of around 4 ppmv in the same time period neglecting water vapor contributions from air masses in the Asian monsoon region.

4 Conclusions

The observed mean water vapor/methane increase of 0.5 ppmv/20 ppbv between both phases i.e. August and September is statistically correlated with an increase in Asian monsoon surface tracer (MON) by 8.6 percentage points which corresponds to a doubling of air masses in the Ex-LS influenced by the Asian monsoon and the region of southeast Asia and tropical Pacific Ocean. Other surface regions can be neglected as source of the moist air masses in the stratosphere. The doubling of MON is also consistent with observations of increased values of other tropospheric tracers (N_2O, SF_6, CO), which were simultaneously observed (*Müller et al.*, 2016). Our observational results also confirm the model study of *Ploeger et al.* (2013), where a simulated increase of the water vapor from 4.5 to 5.0 ppmv in the Ex-LS is correlated to an increase of the Asian monsoon air contribution of about 10 %. Our observed increase in water vapor is also in accordance with the study by *Vogel et al.* (2016), who found that over the entire monsoon time period from June to October 2012 1.5 ppmv of the water vapor in the northern hemispheric stratosphere at 380 K originates from regions of the AMA including southeast Asia and tropical Pacific Ocean.

Moreover, the flightpath back-trajectories support the influence of the Asian monsoon on the Ex-LS. In phase 2 twice as many trajectories show a tropospheric influence compared to phase 1. The moistening in the Ex-LS is maintained by young air masses transported from the Asian monsoon with a mean concentration of about 12 ppmv. The locations of the LCPs show that the imprint of in-mixed water vapor concentrations occurs most frequently above India and south-east Asia. The crossing of the tropopause in case of Eddy shedding events are displaced to regions of Rossy wave breaking along the subtropical jet in combination with quasi-isentropic transport into the Ex-LS as shown by *Vogel et al.* (2016).

All these measurements and model results contribute to the general picture of influencing the trace gas composition of the extra-tropical lower stratosphere in the northern hemisphere by the Asian monsoon at least for the year of 2012. In particular, this study gives observational evidence of the water vapor transport from the Asian monsoon region to the northern Ex-LS. Depending on the residence time in the lower stratosphere the moist and methane-rich air masses have the potential to impact surface temperatures in the northern hemisphere.

Atmospheric
Chemistry
and Physics
Discussions

Atmospheric
Chemistry
and Physics
Discussions

References

Baker, A. K., T. J. Schuck, C. A. M. Brenninkmeijer, A. Rauthe-Schoch, F. Slemr, P. F. J. van Velthoven, and J. Lelieveld (2012), Estimating the contribution of monsoon-related biogenic production to methane emissions from South Asia using CARIBIC observations, *Geophysical Research Letters*, *39*, L10,813, https://doi.org/10.1029/2012GL051756.

5 Bian, J. C., L. L. Pan, L. Paulik, H. Vomel, H. B. Chen, and D. R. Lu (2012), In situ water vapor and ozone measurements in Lhasa and Kunming during the Asian summer monsoon, *Geophysical Research Letters*, *39*, L19,808, https://doi.org/10.1029/2012GL052996.

Bönisch, H., A. Engel, J. Curtius, T. Birner, and P. Hoor (2009), Quantifying transport into the lowermost stratosphere using simultaneous in-situ measurements of SF6 and CO2, *Atmospheric Chemistry and Physics*, *9*(16), 5905–5919.

Dee, D. P., S. M. Uppala, A. J. Simmons, P. Berrisford, P. Poli, S. Kobayashi, U. Andrae, M. A. Balmaseda, G. Balsamo, P. Bauer, P. Bech-
10 told, A. C. M. Beljaars, L. van de Berg, J. Bidlot, N. Bormann, C. Delsol, R. Dragani, M. Fuentes, A. J. Geer, L. Haimberger, S. B. Healy, H. Hersbach, E. V. Hólm, L. Isaksen, P. Kallberg, M. Koehler, M. Matricardi, A. P. McNally, B. M. Monge-Sanz, J. . J. Morcrette, B. . K. Park, C. Peubey, P. de Rosnay, C. Tavolato, J. . N. Thépaut, and F. Vitart (2011), The ERA-Interim reanalysis: configuration and performance of the data assimilation system, *Quarterly Journal of the Royal Meteorological Society*, *137*(656), 553–597, https://doi.org/10.1002/qj.828.

15 Dethof, A., A. O'Neill, J. M. Slingo, and H. G. J. Smit (1999), A mechanism for moistening the lower stratosphere involving the Asian summer monsoon, *Quarterly Journal of the Royal Meteorological Society*, *125*(556), 1079–1106, https://doi.org/10.1256/smsqj.55601.

Forster, P. M. D., and K. P. Shine (2002), Assessing the climate impact of trends in stratospheric water vapor, *Geophysical Research Letters*, *29*(6), 1086, https://doi.org/10.1029/2001GL013909.

Gettelman, A., P. Hoor, L. L. Pan, W. J. Randel, M. I. Hegglin, and T. Birner (2011), The Extratropical Upper Troposphere and Lower
20 Stratosphere, *Reviews of Geophysics*, *49*, RG3003, https://doi.org/10.1029/2011RG000355.

Hoor, P., H. Fischer, and J. Lelieveld (2005), Tropical and extratropical tropospheric air in the lowermost stratosphere over Europe: A CO-based budget, *Geophysical Research Letters*, *32*(7), L07,802, https://doi.org/10.1029/2004GL022018.

Hegglin, M. I. and Tegtmeier, S. and Anderson, J. and Froidevaux, L. and Fuller, R. and Funke, B. and Jones, A. and Lingenfelser, G. and Lumpe, J. and Pendlebury, D. and Remsberg, E. and Rozanov, A. and Toohey, M. and Urban, J. and von Clarmann, T. and Walker, K. A.
25 and Wang, R. and Weigel, K. (2013), SPARC Data Initiative: Comparison of water vapor climatologies from international satellite limb sounders, *Journal of Geophysical Research: Atmospheres*, *118*(20), 2169-8996, https://doi.org/10.1002/jgrd.50752.

Hsu, C. J., and R. A. Plumb (2000), Nonaxisymmetric thermally driven circulations and upper-tropospheric monsoon dynamics, *Journal of the Atmospheric Sciences*, *57*(9), 1255–1276, https://doi.org/10.1175/1520-0469(2000)057<1255:NTDCAU>2.0.CO;2.

Krebsbach, M., C. Schiller, D. Brunner, G. Günther, M. I. Hegglin, D. Mottaghy, M. Riese, N. Spelten, and H. Wernli (2006), Seasonal cycles
30 and variability of O-3 and H2O in the UT/LMS during SPURT, *Atmospheric Chemistry and Physics*, *6*, 109–125.

Kunz, A., M. Sprenger, and H. Wernli (2015), Climatology of potential vorticity streamers and associated isentropic transport pathways across PV gradient barriers, *Journal of Geophysical Research-atmospheres*, *120*(9), 3802–3821, https://doi.org/10.1002/2014JD022615.

Livesey, N. J., W. G. Read, L. Froidevaux, A. Lambert, G. L. Manney, H. C. Pumphrey, M. L. Santee, M. J. Schwartz, S. Wang, R. E. Cofield, D. T. Cuddy, R. A. Fuller, R. F. Jarnot, J. H. Jiang, B. W. Knosp, P. C. Stek, P. A. Wagner, , and D. L. Wu (2011), EOS MLS Version 3.3
35 Level 2 data quality and description document, *Tech. Rep. JPL D33509*, Jet Propulsion Laboratory, available from http://mls.jpl.nasa.gov.

McKenna, D. S., P. Konopka, J. U. Grooß, G. Günther, R. Müller, R. Spang, D. Offermann, and Y. Orsolini (2002a), A new Chemical Lagrangian Model of the Stratosphere (CLaMS) - 1. Formulation of advection and mixing, *Journal of Geophysical Research-atmospheres*, *107*(D16), 4309, https://doi.org/10.1029/2000JD000114.

McKenna, D. S., J. U. Grooß, G. Günther, P. Konopka, R. Müller, G. Carver, and Y. Sasano (2002b), A new Chemical Lagrangian Model of the Stratosphere (CLaMS) - 2. Formulation of chemistry scheme and initialization, *Journal of Geophysical Research-atmospheres*, *107*(D15), 4256, https://doi.org/10.1029/2000JD000113.

Meyer, J., C. Rolf, C. Schiller, S. Rohs, N. Spelten, A. Afchine, M. Zöger, N. Sitnikov, T. D. Thornberry, A. W. Rollins, Z. Bozoki, D. Tatrai, V. Ebert, B. Kühnreich, P. Mackrodt, O. Möhler, H. Saathoff, K. H. Rosenlof, and M. Krämer (2015), Two decades of water vapor measurements with the FISH fluorescence hygrometer: a review, *Atmospheric Chemistry and Physics*, *15*(14), 8521–8538, https://doi.org/10.5194/acp-15-8521-2015.

Müller, S., P. Hoor, H. Bozem, E. Gute, B. Vogel, A. Zahn, H. Bönisch, T. Keber, M. Krämer, C. Rolf, M. Riese, H. Schlager, and A. Engel (2016), Impact of the Asian monsoon on the extratropical lower stratosphere: trace gas observations during TACTS over Europe 2012, *Atmospheric Chemistry and Physics*, *16*(16), 10,573–10,589, https://doi.org/10.5194/acp-16-10573-2016.

Pan, L. L., S. B. Honomichl, D. E. Kinnison, M. Abalos, W. J. Randel, J. W. Bergman, and J. Bian (2016), Transport of chemical tracers from the boundary layer to stratosphere associated with the dynamics of the Asian summer monsoon, *Journal of Geophysical Research-atmospheres*, *121*(23), 14,159–14,174, https://doi.org/10.1002/2016JD025616.

Park, M., W. J. Randel, D. E. Kinnison, R. R. Garcia, and W. Choi (2004), Seasonal variation of methane, water vapor, and nitrogen oxides near the tropopause: Satellite observations and model simulations, *Journal of Geophysical Research-atmospheres*, *109*(D3), D03,302, https://doi.org/10.1029/2003JD003706.

Park, M., W. J. Randel, A. Gettelman, S. T. Massie, and J. H. Jiang (2007), Transport above the Asian summer monsoon anticyclone inferred from Aura Microwave Limb Sounder tracers, *Journal of Geophysical Research-atmospheres*, *112*(D16), D16,309, https://doi.org/10.1029/2006JD008294.

Patra, P. K., Y. Niwa, T. J. Schuck, C. A. M. Brenninkmeijer, T. Machida, H. Matsueda, and Y. Sawa (2011), Carbon balance of South Asia constrained by passenger aircraft CO2 measurements, *Atmospheric Chemistry and Physics*, *11*(9), 4163–4175, https://doi.org/10.5194/acp-11-4163-2011.

Ploeger, F., G. Günther, P. Konopka, S. Fueglistaler, R. Müller, C. Hoppe, A. Kunz, R. Spang, J. U. Grooß, and M. Riese (2013), Horizontal water vapor transport in the lower stratosphere from subtropics to high latitudes during boreal summer, *Journal of Geophysical Research-atmospheres*, *118*(14), 8111–8127, https://doi.org/10.1002/jgrd.50636.

Ploeger, F., C. Gottschling, S. Griessbach, J. U. Grooß, G. Günther, P. Konopka, R. Müller, M. Riese, F. Stroh, M. Tao, J. Ungermann, B. Vogel, and M. von Hobe (2015), A potential vorticity-based determination of the transport barrier in the Asian summer monsoon anticyclone, *Atmospheric Chemistry and Physics*, *15*(22), 13,145–13,159, https://doi.org/10.5194/acp-15-13145-2015.

Pommrich, R., R. Müller, J. U. Grooß, P. Konopka, F. Ploeger, B. Vogel, M. Tao, C. M. Hoppe, G. Günther, N. Spelten, L. Hoffmann, H. C. Pumphrey, S. Viciani, F. D'Amato, C. M. Volk, P. Hoor, H. Schlager, and M. Riese (2014), Tropical troposphere to stratosphere transport of carbon monoxide and long-lived trace species in the Chemical Lagrangian Model of the Stratosphere (CLaMS), *Geoscientific Model Development*, *7*(6), 2895–2916, https://doi.org/10.5194/gmd-7-2895-2014.

Popovic, J. M., and R. A. Plumb (2001), Eddy shedding from the upper-tropospheric Asian monsoon anticyclone, *Journal of the Atmospheric Sciences*, *58*(1), 93–104, https://doi.org/10.1175/1520-0469(2001)058<0093:ESFTUT>2.0.CO;2.

Atmospheric
Chemistry
and Physics
Discussions

Randel, W. J., and M. Park (2006), Deep convective influence on the Asian summer monsoon anticyclone and associated tracer vari-
ability observed with Atmospheric Infrared Sounder (AIRS), *Journal of Geophysical Research-atmospheres*, *111*(D12), D12,314,
https://doi.org/10.1029/2005JD006490.

Riese, M., F. Ploeger, A. Rap, B. Vogel, P. Konopka, M. Dameris, and P. Forster (2012), Impact of uncertainties in atmospheric mix-
ing on simulated UTLS composition and related radiative effects, *Journal of Geophysical Research-atmospheres*, *117*, D16,305,
https://doi.org/10.1029/2012JD017751.

Santee, M. L., G. L. Manney, N. J. Livesey, M. J. Schwartz, J. L. Neu, and W. G. Read (2017), A comprehensive overview of the climatological
composition of the Asian summer monsoon anticyclone based on 10 years of Aura Microwave Limb Sounder measurements, *Journal of
Geophysical Research: Atmospheres*, *122*(10), 5491–5514, https://doi.org/10.1002/2016JD026408, 2016JD026408.

Schoeberl, M. R., and A. E. Dessler (2011), Dehydration of the stratosphere, *Atmospheric Chemistry and Physics*, *11*(16), 8433–8446,
https://doi.org/10.5194/acp-11-8433-2011.

Schuck, T. J., C. A. M. Brenninkmeijer, A. K. Baker, F. Slemr, P. F. J. von Velthoven, and A. Zahn (2010), Greenhouse gas relationships in the
Indian summer monsoon plume measured by the CARIBIC passenger aircraft, *Atmospheric Chemistry and Physics*, *10*(8), 3965–3984.

Uma, K. N., S. K. Das, and S. S. Das (2014), A climatological perspective of water vapor at the UTLS region over differ-
ent global monsoon regions: observations inferred from the Aura-MLS and reanalysis data, *Climate Dynamics*, *43*(1-2), 407–420,
https://doi.org/10.1007/s00382-014-2085-9.

Vogel, B., G. Günther, R. Müller, J. U. Grooß, P. Hoor, M. Krämer, S. Müller, A. Zahn, and M. Riese (2014), Fast transport from Southeast
Asia boundary layer sources to northern Europe: rapid uplift in typhoons and eastward eddy shedding of the Asian monsoon anticyclone,
Atmospheric Chemistry and Physics, *14*(23), 12,745–12,762, https://doi.org/10.5194/acp-14-12745-2014.

Vogel, B., G. Günther, R. Müller, J. U. Grooß, and M. Riese (2015), Impact of different Asian source regions on the composition of the
Asian monsoon anticyclone and of the extratropical lowermost stratosphere, *Atmospheric Chemistry and Physics*, *15*(23), 13,699–13,716,
https://doi.org/10.5194/acp-15-13699-2015.

Vogel, B., G. Günther, R. Müller, J. U. Grooß, A. Afchine, H. Bozem, P. Hoor, M. Krämer, S. Müller, M. Riese, C. Rolf, N. Spelten,
G. P. Stiller, J. Ungermann, and A. Zahn (2016), Long-range transport pathways of tropospheric source gases originating in Asia into
the northern lower stratosphere during the Asian monsoon season 2012, *Atmospheric Chemistry and Physics*, *16*(23), 15,301–15,325,
https://doi.org/10.5194/acp-16-15301-2016.

Xiong, X., S. Houweling, J. Wei, E. Maddy, F. Sun, and C. Barnet (2009), Methane plume over south Asia during the monsoon season:
satellite observation and model simulation, *Atmospheric Chemistry and Physics*, *9*(3), 783–794.

Zahn, A., E. Christner, P. F. J. van Velthoven, A. Rauthe-Schoch, and C. A. M. Brenninkmeijer (2014), Processes controlling water vapor
in the upper troposphere/lowermost stratosphere: An analysis of 8years of monthly measurements by the IAGOS-CARIBIC observatory,
Journal of Geophysical Research-atmospheres, *119*(19), 11,505–11,525, https://doi.org/10.1002/2014JD021687.

Zöger, M., A. Afchine, N. Eicke, M. T. Gerhards, E. Klein, D. S. McKenna, U. Morschel, U. Schmidt, V. Tan, F. Tuitjer, T. Woyke, and
C. Schiller (1999), Fast in situ stratospheric hygrometers: A new family of balloon-borne and airborne Lyman alpha photofragment
fluorescence hygrometers, *Journal of Geophysical Research-atmospheres*, *104*(D1), 1807–1816, https://doi.org/10.1029/1998JD100025.
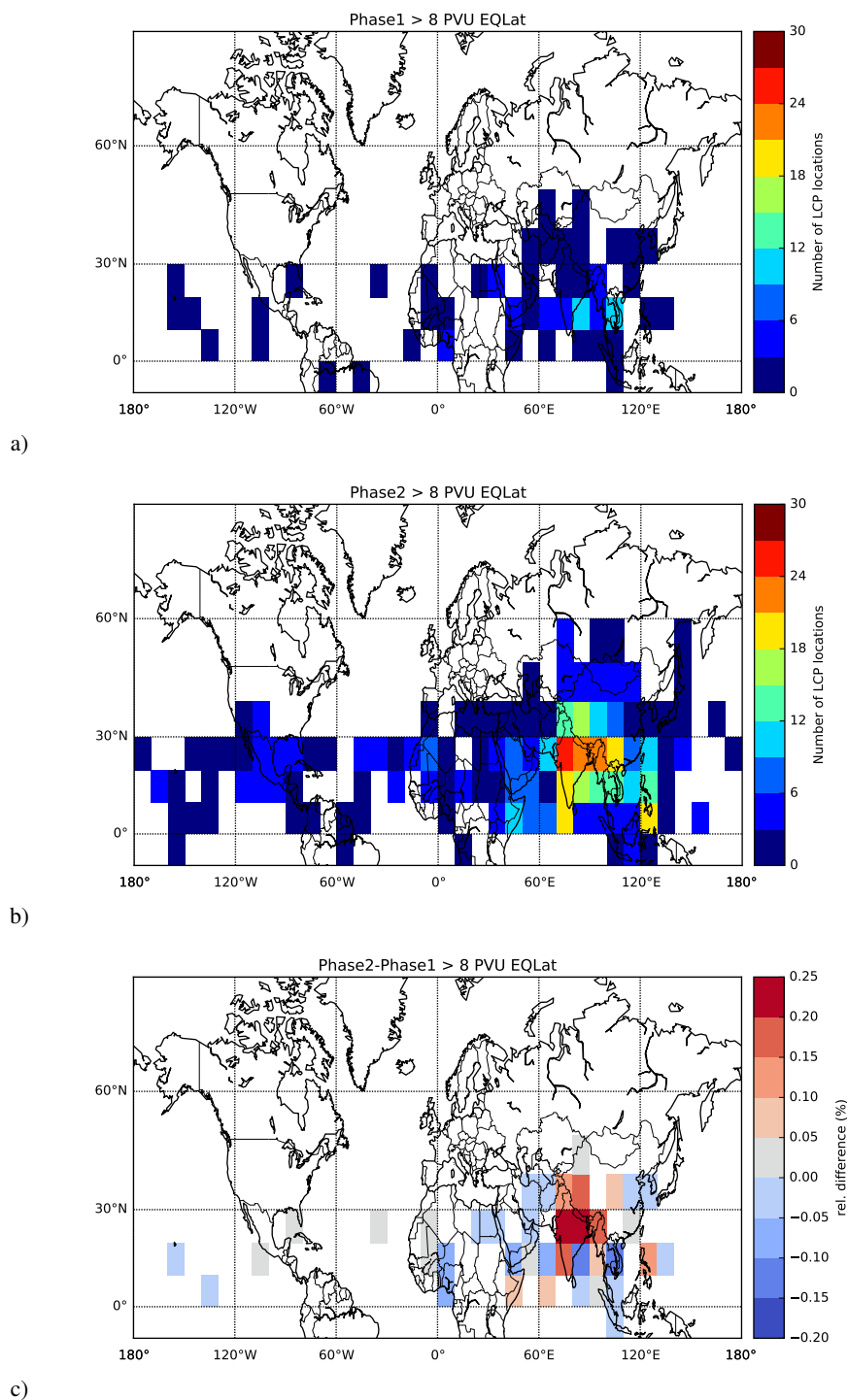
Figure 4. Location of Lagrangian Cold point (LCP) binned by longitude and latitude. LCP location for phase 1 and phase 2 are shown in a) and b), respectively. The relative difference normalized to the total number of trajectories is shown in Fig. c).
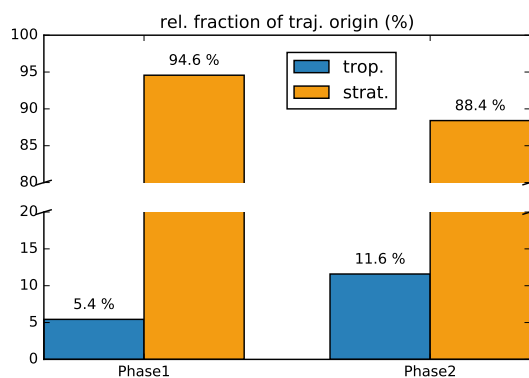
Figure 5. Fraction of trajectories with tropospheric (blue) or stratospheric (orange) origin for each phase.